International Journal of Applied Earth Observation and Geoinformation xxx (2010) xxx–xxx

Contents lists available at ScienceDirect

International Journal of Applied Earth Observation and Geoinformation

journal homepage: www.elsevier.com/locate/jag

Mexico City subsidence observed with persistent scatterer InSAR

Batuhan Osmanoğlu [a,*], Timothy H. Dixon [a], Shimon Wdowinski [a], Enrique Cabral-Cano [b], Yan Jiang [a]

[a] Division of Marine Geology and Geophysics, University of Miami, 4600 Rickenbacker Causeway, Miami, FL 33149-1098, United States
[b] Departamento de Geomagnetismo y Exploración, Instituto de Geofísica, Universidad Nacional Autónoma de México, Ciudad Universitaria, México, D.F. 04510, Mexico

ARTICLE INFO

Article history:
Received 17 November 2009
Accepted 28 May 2010

Keywords:
Subsidence
Interferometry
GPS
Mexico City
Synthetic aperture radar (SAR)
interferometry
Persistent scatterer interferometry (PSI)

ABSTRACT

We analyzed 23 satellite SAR (synthetic aperture radar) scenes using Persistent Scatter Interferometry (PSI) to study subsidence in Mexico City associated with groundwater withdrawal. The data were acquired by the Envisat ASAR system between January 2004 and July 2006. The spatial pattern of subsidence and the maximum subsidence rate (300 mm/year) are similar to earlier studies. Comparison to independent GPS data indicates RMS agreement between the two techniques of 6.9 mm/year, about the level expected based on joint data uncertainty. Significant annual variation in the GPS vertical data is not observed, suggesting minimal aquifer recharge during the rainy season, and justifying a simple linear model of phase variation through time for the PSI analysis.

1. Introduction

The eastern portion of Mexico City is undergoing rapid subsidence due to extraction of ground water in excess of natural recharge and consequent compaction of clay-rich lacustrine sediment (Gayol, 1929; Cuevas, 1936; Carrillo, 1947; Ortega-Guerrero et al., 1993). Interferometric SAR (InSAR) studies (Strozzi and Wegmuller, 1999; Cabral-Cano et al., 2008) have shown subsidence rates as high as 37 cm/year, and document the spatial variation of subsidence, which is closely related to the boundaries of ancient Lake Texcoco, and the thickness of underlying infill basin sediments.

While the existing InSAR studies show much greater spatial detail compared to previous subsidence studies (based on terrestrial leveling surveys), they nevertheless lack the spatial resolution to perform risk assessment for individual structures in the urban environment associated with differential subsidence. Moreover, they lack the temporal resolution to study seasonal to annual variation in subsidence. The timing and amplitude of potential oscillations are important for understanding the ground water hydrology of the Basin of Mexico and managing its aquifer system, and will depend on variables such as the amount and seasonality of water flux (discharge and recharge), and the type, porosity and permeability of the sediment (Freeze and Cherry, 1979) For example seasonal uplift associated with wet season recharge would suggest that the aquifer retains an elastic component of deformation despite long-term decline, and hence has the potential to recover some storage capability under enhanced future management (Terzaghi, 1976; Freeze and Cherry, 1979; Amelung et al., 1999).

In contrast to standard SAR interferometry, persistent scatterer InSAR (PSI) provides a time series of displacement for individual radar scatterers, in principle allowing us to investigate temporal variation in the subsidence pattern, and better understand the behavior and characteristics of the aquifer system. In addition, by focusing on the persistent scatters, we can enhance the effective spatial resolution of deformation maps, revealing critical spatial details that are not observable with standard InSAR. On the other hand PSI analysis can be challenging in areas with high fringe rate (deformation gradient) such as those exhibited in our study area. In this paper we present the first PSI analysis in Mexico City. We use 23 Envisat scenes processed with the PSI technique and nine continuous GPS (C-GPS) stations to investigate temporal and spatial variation of subsidence in Mexico City between early 2004 and mid-2006. C-GPS stations located inside the PSI study area are used to distinguish horizontal and vertical components of deformation, assess temporal variation, and validate the PSI observations.

2. Data analysis

2.1. GPS

Fig. 1 shows the extent of the study area along with the locations of analyzed continuous GPS (C-GPS) stations. There are nine

* Corresponding author. Tel.: +1 305 421 4928.
E-mail addresses: batu@rsmas.miami.edu, batuhan.osmanoglu@gmail.com (B. Osmanoğlu).

0303-2434/$ – see front matter © 2010 Elsevier B.V. All rights reserved.
doi:10.1016/j.jag.2010.05.009

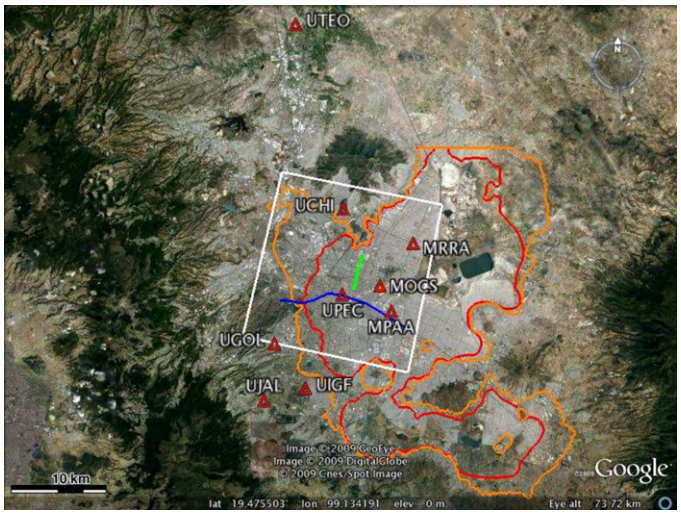

Fig. 1. Outline of PSI study area (white box) and GPS sites used for validation (red triangles). Locations discussed in text and subsequent figures include: Subway Metro Line 4 (green line), a geologic cross section (blue line), and Metropolitan Cathedral (adjacent to UPEC GPS station). The lacustrine and transitional geotechnical units are mapped by the red and orange outlines respectively. (For interpretation of the references to color in this figure legend, the reader is referred to the web version of the article.)

Table 1
Velocity data for Continuous GPS (point-positioning solutions, ITRF 2000).

Station	*N* [mm/year]	*E* [mm/year]	*V* [mm/year]
MOCS	19.6 ± 0.5	−10.0 ± 0.6	−171.6 ± 1.2
MPAA	−2.7 ± 1.3	1.5 ± 4.2	−223.2 ± 4.2
MRRA	−7.5 ± 0.5	−5.9 ± 1.0	−274.1 ± 1.6
UCHI	−6.1 ± 0.5	−7.4 ± 0.9	5.8 ± 1.8
UGOL	−4.2 ± 1.4	−5.1 ± 2.7	1.7 ± 6.0
UIGF	−6.5 ± 0.3	−8.8 ± 0.7	−0.6 ± 1.1
UJAL	−9.2 ± 0.6	−8.9 ± 1.0	3.0 ± 1.8
UPEC	−2.2 ± 0.6	−6.0 ± 2.1	−103.2 ± 6.0
UTEO	−5.7 ± 0.3	−6.6 ± 0.5	−8.2 ± 1.0

continuous GPS stations in or near the study area. Four of these stations (MOCS, MPAA, MRRA and UPEC) are located within the subsidence-prone lacustrine zone (Gobierno del Distrito Federal, 2004). UCHI and UIGF are located on volcanic domes and basaltic lava flows respectively, while UGOL, UJAL and UTEO are located on tephra deposits. GPS data were processed using GIPSY-OASIS software from Jet Propulsion Laboratory (JPL) (Webb and Zumberge, 1997) for precise point positioning using the ITRF-2000 reference frame (Altamimi et al., 2002; Argus, 2007). Details of the procedures and estimation of uncertainties for GPS measurements are described in Dixon et al. (2000) and Sella et al. (2002). We present data in both "absolute" coordinates (latitude, longitude, and height) as well as baseline solutions (Tables 1 and 2, Figs. 2 and 3). In this latter format the position data are referenced to a nearby base station (UCHI). Baseline data exhibit less scatter relative to absolute coordinate data, due to reduction of common mode errors (described below). Baseline data are only available for the period of time that the UCHI time series exist (Fig. 4).

Table 2
Velocity data for Continuous GPS station relative to UCHI.

Station	*N* [mm/year]	*E* [mm/year]	*V* [mm/year]
MOCS	23.3 ± 0.9	−0.4 ± 1.4	−179.9 ± 2.8
MPAA	2.7 ± 2.1	5.0 ± 7.1	−233.5 ± 0.9
MRRA	−3.1 ± 0.8	1.9 ± 2.2	−285.3 ± 3.3
UGOL	1.1 ± 1.0	2.0 ± 2.5	−6.1 ± 5.4
UIGF	−2.1 ± 0.5	0.4 ± 1.0	−10.0 ± 2.1
UJAL	−1.0 ± 0.9	0.8 ± 2.4	0.8 ± 3.9
UPEC	0.1 ± 1.4	−0.1 ± 3.0	−78.7 ± 8.7
UTEO	0.5 ± 1.2	2.2 ± 3.0	−8.3 ± 7.1

Several noise sources might effect the GPS measurements. Due to the small size of the study area, orbital effects can be assumed spatially uniform, and hence will largely cancel in the baseline solutions. Transient deformation generated along the Oaxaca and Guerrero segments of the Mid America Trench extend inland and have been observed in the Mexico City GPS network (Correa-Mora et al., 2008, 2009). Effects of this transient deformation are also minimized using the baseline approach. UCHI was selected as the master site for all baseline calculations because it has the longest time series among the GPS sites located on stable ground in the study area. UCHI is located within the Sierra de Guadalupe, a large andesitic-dacitic structure on the northern edge of the city. Also, by selecting a stable reference GPS site within the PSI study area, we can tie the relative PSI solutions to GPS and directly compare radar line-of-sight (LOS) and GPS velocities. We project the GPS measurements to the LOS vector as follows:

$$\mathrm{GPS_{los}} = \mathrm{GPS_{north}} \times (-1) \times \cos\left(\gamma - \frac{3\pi}{2}\right) \times \sin(\theta) + \mathrm{GPS_{east}} \times (-1) \times \sin\left(\gamma - \frac{3\pi}{2}\right) \times \sin(\theta) + \mathrm{GPS_{up}} \times \cos(\theta) \quad (1)$$

where γ indicates the satellite's orbit angle relative to true north and θ indicates the incidence angle of the radar wave (Hanssen, 2001). As shown in Fig. 2 the most significant positioning changes occur in the vertical component and are characterized by a steep linear trend (MOCS, MPAA, MRRA, and UPEC) with negligible seasonal variation. Therefore, we used a linear model for PSI analysis and construction of the LOS time series from the SAR data. Justification for the linear model is discussed in more detail in Section 3.2.

2.2. SAR analysis

Twenty-three Envisat scenes acquired between January 2004 and July 2006 were used to generate interferograms with DORIS (Delft Object-oriented Radar Interferometry Software) (Kampes and Usai, 1999). Precise orbits from the Delft Institute were used to minimize orbital errors (Scharroo and Visser, 1998). The 29 July 2005 acquisition is selected as the master scene to minimize the effects of spatial and temporal baselines (Fig. 4) (Zebker and Villasensor, 1992; Kampes and Usai, 1999) Temporal, spatial and Doppler baselines are listed in Table 3. The study area is about 20 km × 20 km and is centered over the Mexico City historic downtown. The study area is cropped from each acquisition and oversampled by a factor of two in range and azimuth to avoid undersampling of the interferogram, especially during resampling of the slave acquisition (Hanssen and Bamler, 1999).

Time-series analysis using SAR interferometry is a recent technology exploiting the phase history of strong scatterers (e.g. Ferretti et al., 2001; Hooper et al., 2004; Lanari et al., 2004; Kampes, 2005; Gourmelen et al., 2007). It is based on a stack of interferograms relative to a single master image. The algorithm starts with selecting strong scatterers visible in all interferograms and unwrapping their phase changes through time (Ferretti et al., 2001). These strong scatterers are further filtered to detect and remove the atmospheric phase contribution, commonly referred as the atmospheric phase screen (APS). Eq. (2) shows major factors influencing the InSAR phase (ϕ) measurements (Hanssen, 2001):

$$\phi = \phi_{def} + \phi_{topo} + \phi_{orbit} + \phi_{aps} + \phi_{scat} + \phi_{noise} \quad (2)$$

where the subscripts define the individual factors or noise sources influencing the phase measurement, e.g., ϕ_{def} is the deformation

Please cite this article in press as: Osmanoğlu, B., et al., Mexico City subsidence observed with persistent scatterer InSAR. Int. J. Appl. Earth Observ. Geoinf. (2010), doi:10.1016/j.jag.2010.05.009

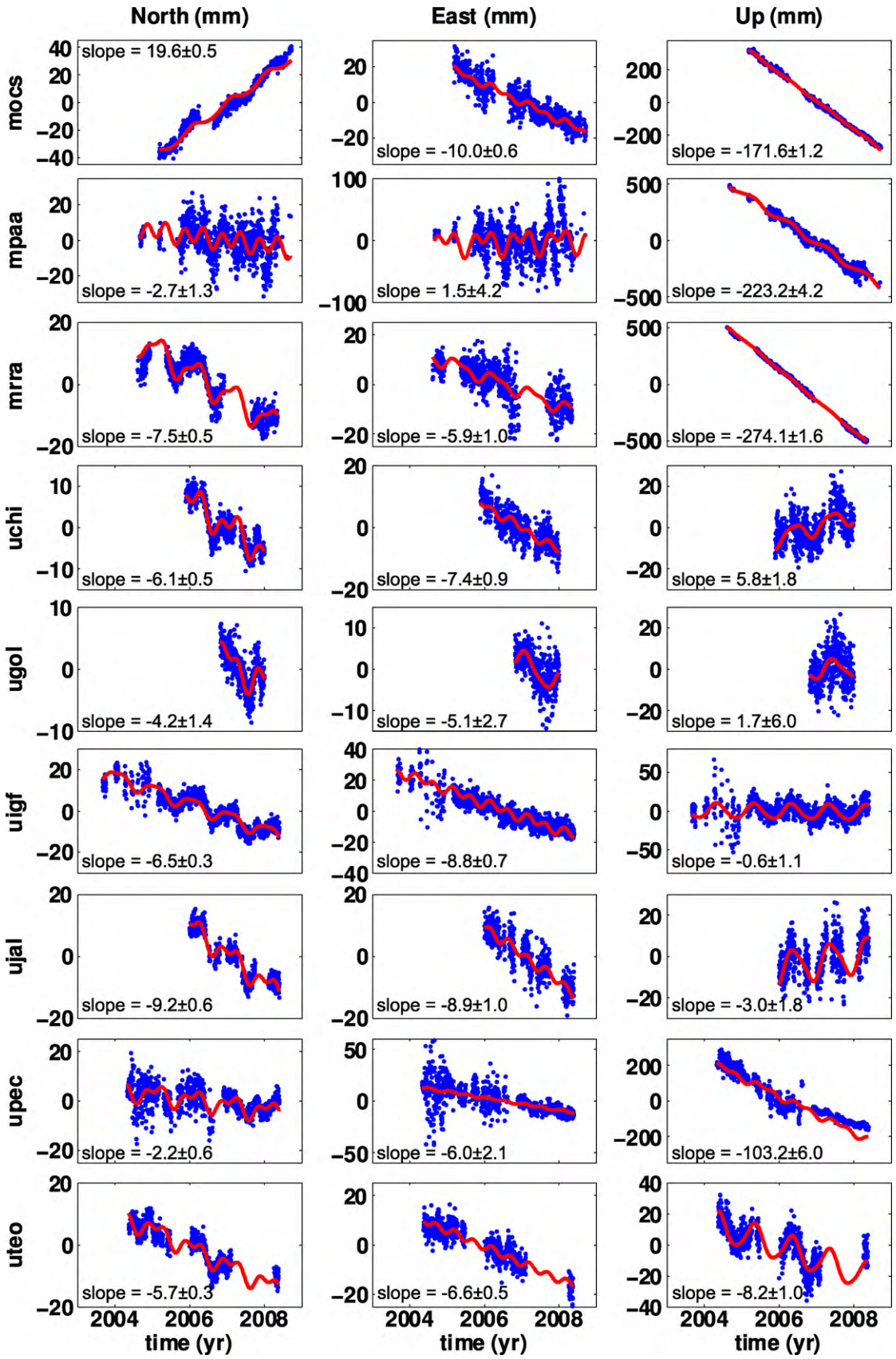

Fig. 2. North, East and Vertical components of motion observed by the permanent GPS stations using point positioning and the ITRF-2000 reference frame. Note the rapid subsidence observed at some stations.

Please cite this article in press as: Osmanoğlu, B., et al., Mexico City subsidence observed with persistent scatterer InSAR. Int. J. Appl. Earth Observ. Geoinf. (2010), doi:10.1016/j.jag.2010.05.009

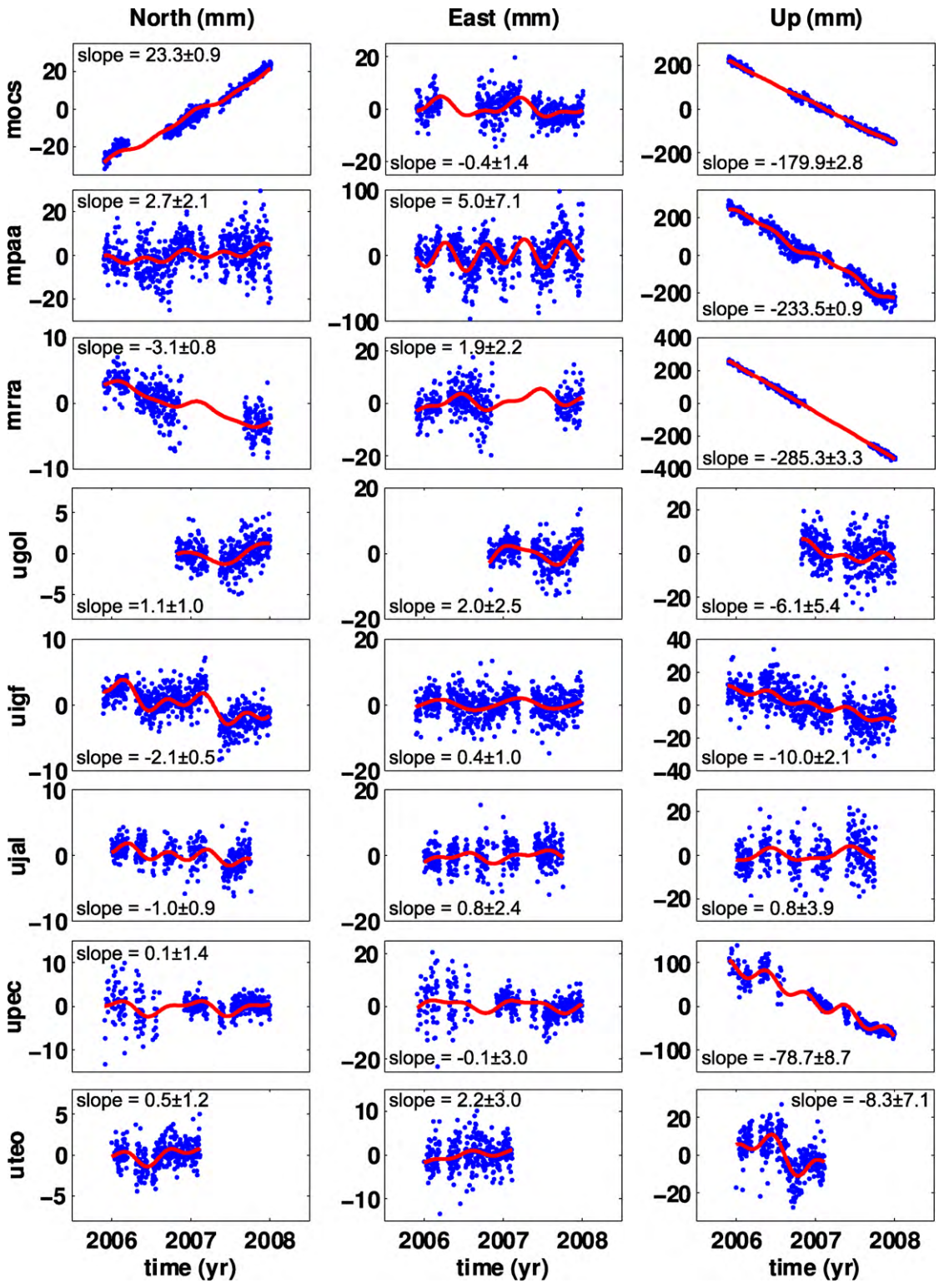

Fig. 3. Similar to Fig. 2 using baseline solutions for the GPS data using UCHI as master GPS station.

signal of interest, ϕ_{topo} is the topographic phase contribution or digital elevation model (DEM) error and ϕ_{orbit} is the contribution due to orbital errors, believed to be minimal with the use of precise orbits. APS (ϕ_{aps}) is the phase contribution due to the atmospheric phase screen. Phase response of a persistent scatterer does not change over time, therefore (ϕ_{scat}) can be ignored. For strong scatterers the effect of phase noise (ϕ_{noise}) is negligible. Accurate geolocations of PSI scatterers are calculated using the corrected DEM. Fig. 5 shows the LOS subsidence rates derived from PSI.

In this paper PSI results are overlaid on Google Earth imagery. A small misfit in the location of the PSI points is evident around tall buildings where the SAR look direction differs substantially from the optical viewing angle. For PSI the data are oversampled by a factor of two in range and azimuth making each resolution cell half the size of single-look complex radar pixel (4 m × 20 m), i.e., approxi-

Please cite this article in press as: Osmanoğlu, B., et al., Mexico City subsidence observed with persistent scatterer InSAR. Int. J. Appl. Earth Observ. Geoinf. (2010), doi:10.1016/j.jag.2010.05.009

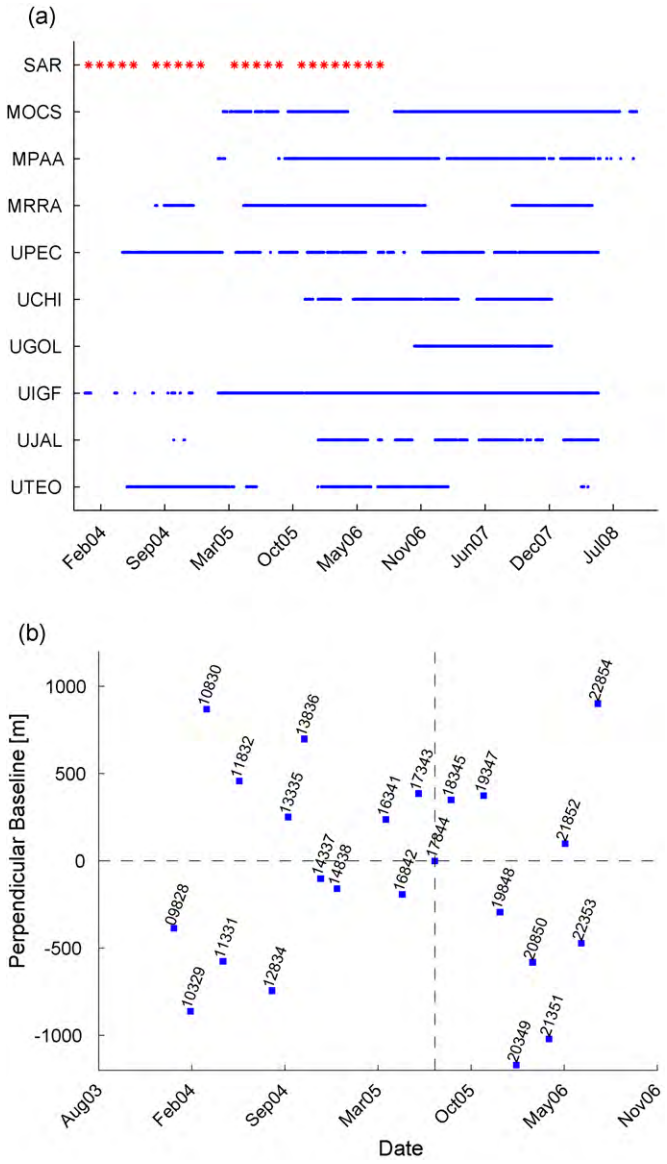

Fig. 4. (a) Time-span of available data from continuous GPS stations (blue lines) and InSAR (red stars). (b) Perpendicular and temporal baselines for PSI, labeled with the orbit number of acquisition. Detailed information is in Table 3. (For interpretation of the references to color in this figure legend, the reader is referred to the web version of the article.)

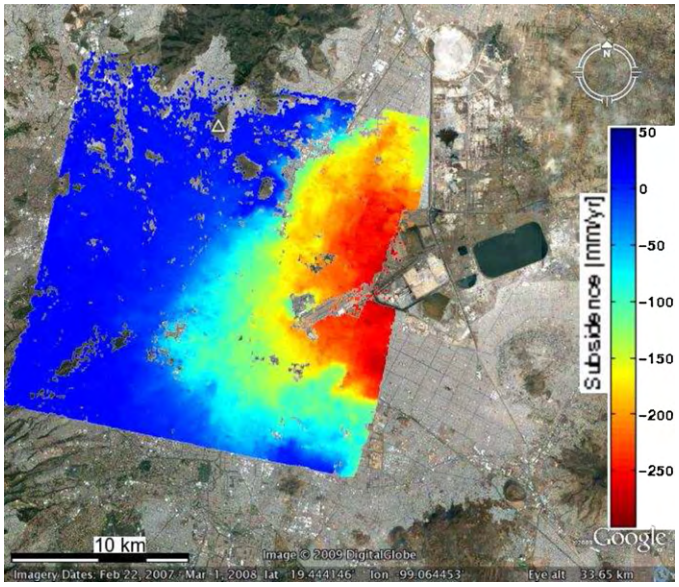

Fig. 5. PSI results showing subsidence through part of Mexico City. Maximum rate (300 mm/year) occurs in eastern Mexico City and the gradient of subsidence increases towards the remnant of Lake Texcoco (dark rectangle). Master PSI point (white triangle) is located 454.5 m away from UCHI GPS station, on a remnant volcanic hill.

mately 2 m × 10 m. The geolocation accuracy for standard Envisat processing with DORIS precise orbits, which is based on a reference ellipsoid, is about 3 pixels in both range and azimuth directions corresponding to about 12 m in azimuth by 60 m in range (Small et al., 2004). In this study we improve the geolocation accuracy by using SRTM 3 arcsec data combined with the topographic heights calculated from the PSI. Therefore in the final product the geocoding error is less than 10 m in azimuth direction and is less than 15 m in the range direction (Hong et al., 2004).

3. Results and discussion

3.1. GPS Results

GPS results are presented in Tables 1, 2 and 6 and Figs. 2, 3 and 6 GPS data indicate that the eastern sector of Mexico City is subsiding at high rates. Rates presented in this study are in agreement with earlier publications (Cabral-Cano et al., 2008). Horizontal components of the GPS time series are affected by both regional tectonics and local surface motion that might be due to ground

Table 3
Baseline information for Envisat ASAR data.

Date	B.Perp[a] [m]	B.Temp[b] [days]	B.Dopp[c] [Hz]	Date	B.Perp[a] [m]	B.Temp[b] [days]	B.Dopp[c] [Hz]
16 January 2004	−386.2	−560	−0.3	24 June 2005	386.3	−35	5.6
20 February 2004	−862	−525	6.4	29 July 2005[d]	0	0	0
26 March 2004	869.9	−490	5.9	02 September 2005	350.1	35	−1.6
30 April 2004	−575.7	−455	2.5	11 November 2005	374.3	105	20.0
04 June 2004	458.8	−420	1.0	16 December 2005	−292.5	140	20.0
13 August 2004	−743.8	−350	6.7	20 January 2006	−1170.3	175	19.9
17 September 2004	251.6	−315	7.0	24 February 2006	−580.8	210	21.5
22 October 2004	698.9	−280	6.9	31 March 2006	−1019.3	245	26.4
26 November 2004	−101.3	−245	3.0	05 May 2006	98.2	280	27.7
31 December 2004	−158.7	−210	0.6	09 June 2006	−472.1	315	23.4
15 April 2005	237.8	−105	7.9	14 July 2006	901.8	350	26.5
20 May 2005	−191.2	−70	0.3				

[a] B.Perp Perpendicularbaseline between orbits of the master and slave scenes.
[b] B.Temp Temporal baseline (time difference) between master and slave acquisitions.
[c] B.Dopp The difference between the Doppler centroid frequencies of master and slave scenes.
[d] Master scene.

Please cite this article in press as: Osmanoğlu, B., et al., Mexico City subsidence observed with persistent scatterer InSAR. Int. J. Appl. Earth Observ. Geoinf. (2010), doi:10.1016/j.jag.2010.05.009

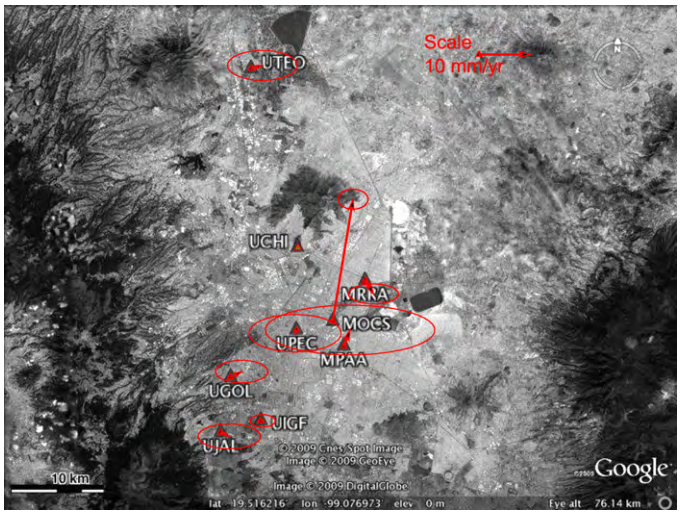

Fig. 6. Horizontal motions of GPS sites relative to UCHI (Table 2).

water extraction. Given the close proximity of the GPS sites to each other, the baseline approach should cancel out most of the tectonic motion. Horizontal motion due to sediment consolidation and shallow faulting is expected to have a concentric pattern centered on the thickest package of compressible sediments, located under the faster subsiding areas (Cabral-Cano et al., 2008). Observed horizontal components of the GPS baseline solutions are plotted in Fig. 6. All sites except for MOCS exhibit horizontal motions that are very small compared to the vertical component, close to the level of uncertainty. MOCS on the other hand shows a clear NNE motion (Table 2). This may be the result of the location of this station on the northern edge of Peñon de los Baños, a volcanic dome structure north of Mexico's International Airport. This motion may reflect detachment of the consolidated sediment package from the surfaces of this topographic feature. We conclude that horizontal surface motion due to sediment consolidation is not significant. The remaining discussion focuses on the vertical component.

3.2. Temporal variation

Subsidence due to ground water extraction in excess of recharge is a world-wide problem in areas that are heavily dependent on the underground water supply (Poland, 1984; Ortega-Guerrero et al., 1993; Amelung et al., 1999; Strozzi et al., 2002; Sneed et al., 2003). The relationship between surface deformation and water extraction can provide important information about subsurface conditions. Sand and gravel layers (aquifers) react to water extraction almost instantaneously and can expand elastically when water is injected back into their pore space. On the other hand compaction of clay and silt rich layers (aquitards) tends to be inelastic. Irreversible aquitard compaction can permanently reduce the capacity for underground water storage (Terzaghi, 1976). In aquitards, when currently applied stresses due to extraction are stronger than the preconsolidation stress (the stress prior to water pumping), soil particles rearrange to carry the additional load, and may undergo weak chemical bonding, leading to irreversible compaction (Sneed et al., 2003).

The presence of annual and seasonal signals in areas that are subsiding due to ground water extraction can indicate aquifer recharge. Annual or seasonal uplift may occur in response to natural recharge associated with the rainy season and would also be reflected as a change in hydraulic head. Such observations are important in reservoir management because they would indicate that the aquifer maintains some capacity to regain storage capability. We initially began this study in order to investigate possible annual and seasonal signals in the PSI data. However inspection of our GPS data indicates that annual and seasonal signals in the vertical component are small at most sites. Residuals to a linear fit of the PSI time series are also negligible. The amplitudes of the annual term in the GPS baseline range from 1 to 17 mm (mean 4.6 mm), very small compared to the total annual subsidence at many stations (Tables 4 and 5). If the measured surface response to ground water recharge is out-of-phase at different GPS sites, the baseline approach described above can reduce the sensitivity of the dataset to annual signals. We therefore did the same analysis using precise point-positioning solutions (Fig. 7(a)). Results again indicate very small annual oscillations. In summary

Table 4
Annual and semi-annual fit to point-positioning vertical GPS data.

Station	Annual amplitude [mm]	Semi-annual amplitude [mm]	Annual phase[a] [days]	Semi-annual phase[a] [days]
MOCS	4.2	0.7	337.8	100.2
MPAA	26.3	5.7	351.9	60.7
MRRA	6.1	0.8	340.4	49.3
UCHI	4.1	0.8	311.2	178.8
UGOL	4.3	0.6	280.7	37.2
UIGF	9.5	1.9	333.1	99.7
UJAL	8.1	1.8	316.9	120.2
UPEC	13.5	1.7	318.9	101.2
UTEO	9.2	1.2	330.3	76.8

[a] Phase: days past January 1st.

Table 5
Annual and semi-annual fit to baseline vertical GPS data.

Station	Annual amplitude [mm]	Semi-annual amplitude [mm]	Annual phase[a] [days]	Semi-annual phase[a] [days]
MOCS	2.6	1.7	98.6	68.4
MPAA	17.4	9.7	0.5	49.0
MRRA	1.1	1.4	318.3	86.1
UGOL	2.1	1.0	169.2	77.5
UIGF	1.0	2.0	314.8	79.1
UJAL	2.6	1.5	304.6	65.8
UPEC	6.1	4.7	69.2	80.2
UTEO	6.6	5	325.6	51.3

[a] Phase: days past January 1st.

Please cite this article in press as: Osmanoğlu, B., et al., Mexico City subsidence observed with persistent scatterer InSAR. Int. J. Appl. Earth Observ. Geoinf. (2010), doi:10.1016/j.jag.2010.05.009

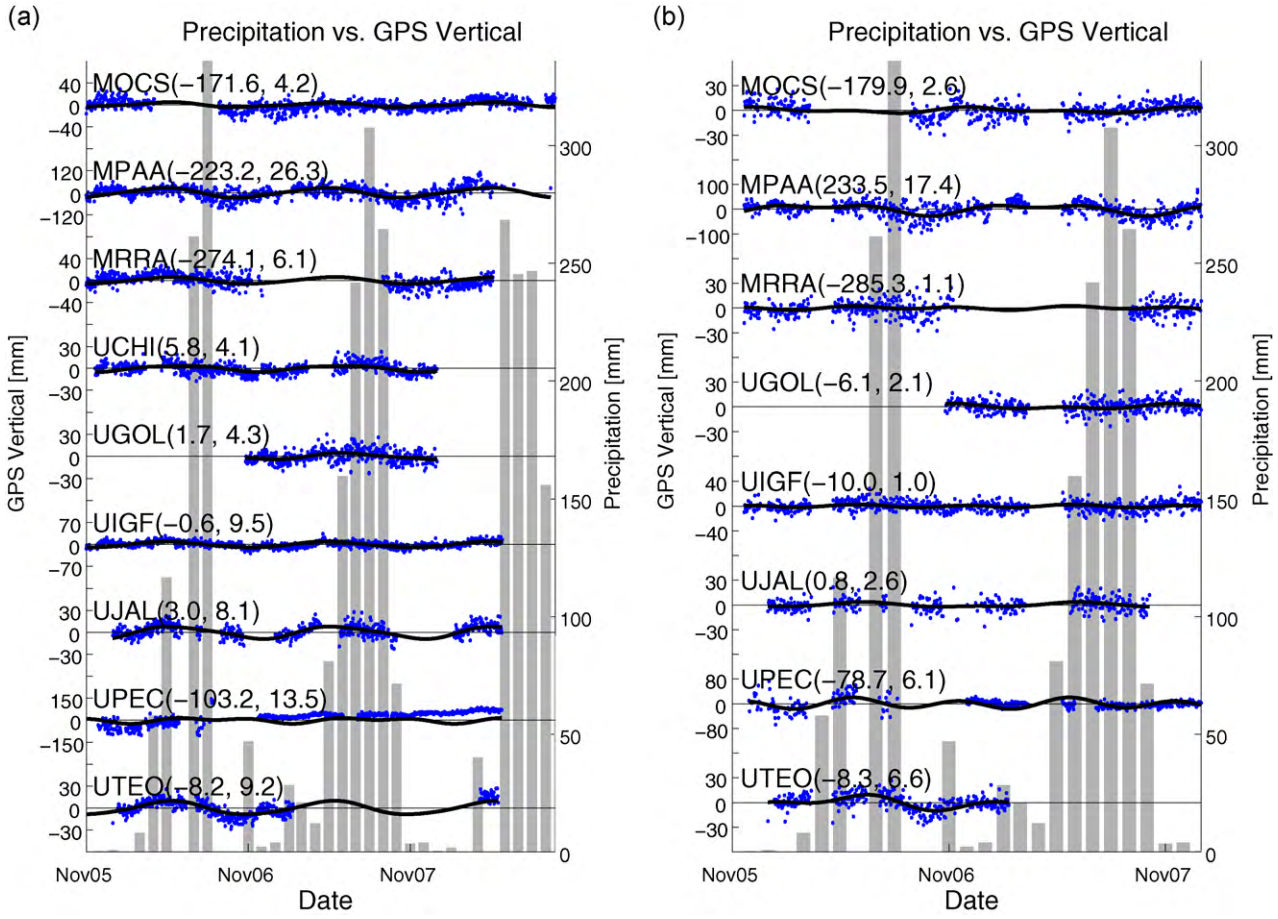

Fig. 7. (a) Detrended GPS vertical point-positioning solutions. The light-gray bars in the background show monthly-average rain data collected at UJAL station. Values in parenthesis after station name indicate the subtracted rate (mm/year), and amplitude (mm) of the annual signal. Black continuous line is the best fitting model, accounting for annual and semi-annual signals. (b) Similar to Fig. 7(a) using detrended baseline GPS solutions for MOCS, MPAA, MRRA and UPEC. Note smaller annual amplitude.

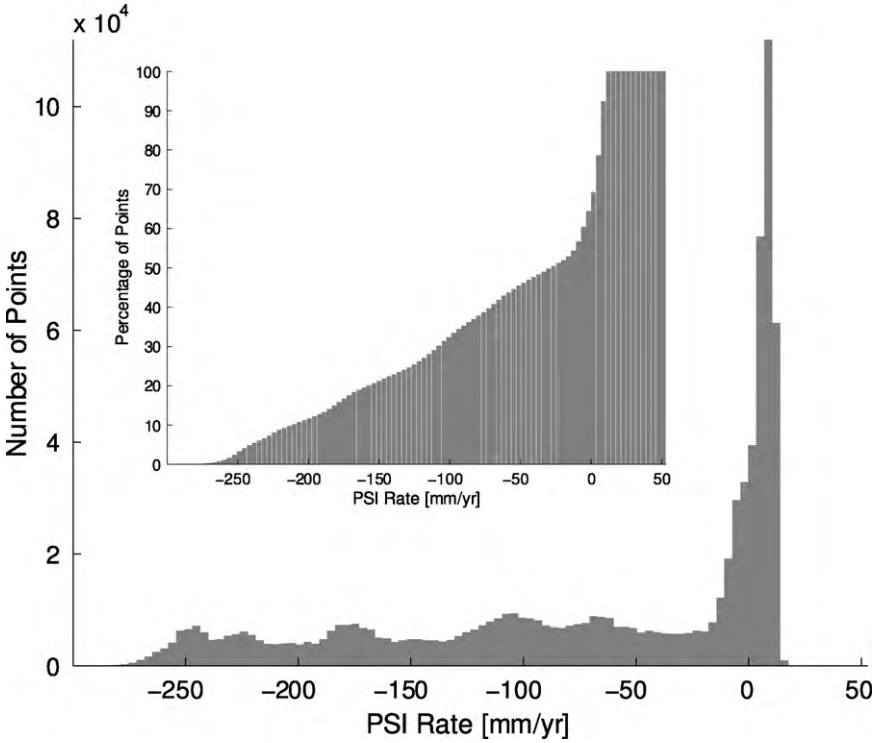

Fig. 8. Histogram of observed PSI subsidence rates. Inset shows cumulative distribution.

Please cite this article in press as: Osmanoğlu, B., et al., Mexico City subsidence observed with persistent scatterer InSAR. Int. J. Appl. Earth Observ. Geoinf. (2010), doi:10.1016/j.jag.2010.05.009

Table 6
LOS rates: GPS vs. PSI.

Site	GPS-point Positioning [mm/year]	GPS-baseline [mm/year]	PSI [mm/year]
MOCS	−149.1	−153.2	−161.5
MPAA	−204.5	−212.0	−207.8
MRRA	−252.8	−260.6	−254.4
UGOL	−1.0	−5.4	−12.8
UPEC	−84.9	−77.1	−84.9
UCHI	2.0	0	0

we see no evidence of significant recharge associated with the rainy season or any other artificial recharge process. Based on the GPS results, the PSI analysis uses a simple linear deformation model.

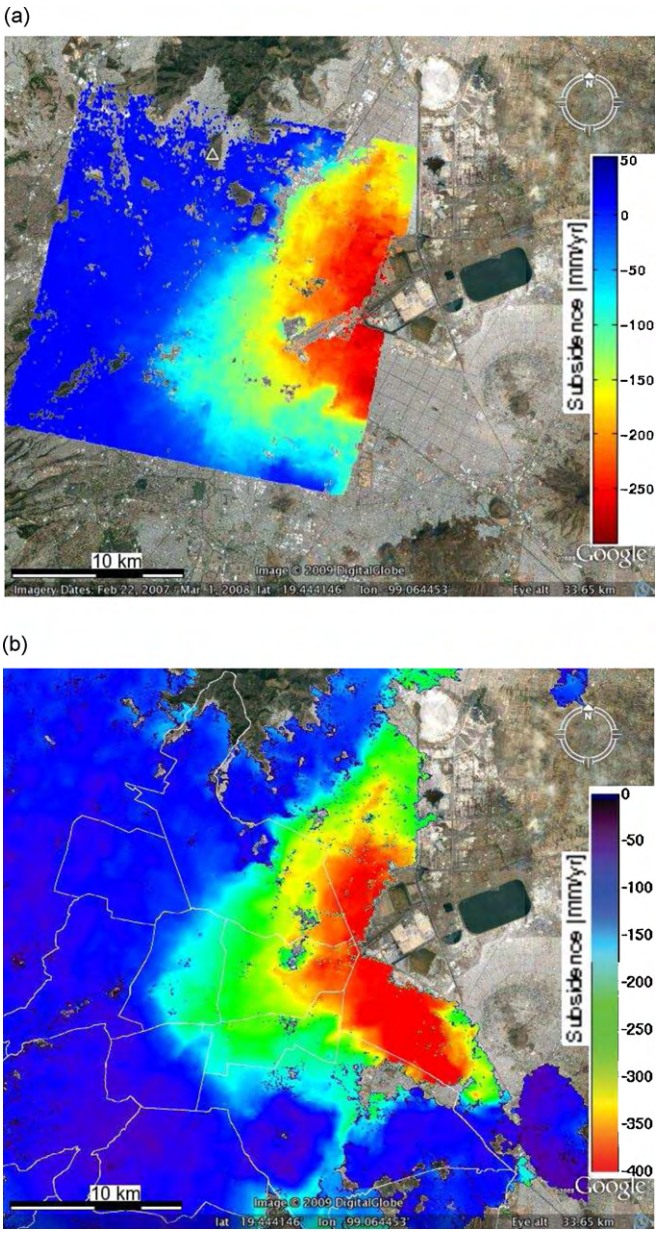

Fig. 9. (a) Subsidence rates for the period 16 January 2004 to 14 July 2006 using Envisat ASAR data (this study). (b) Subsidence rates for the period 16 July 1999 and 7 January 2000 (DInSAR, ERS-2; Cabral-Cano et al., 2008). The subsidence magnitude and pattern are very similar despite being observed at different times and with different analytical techniques.

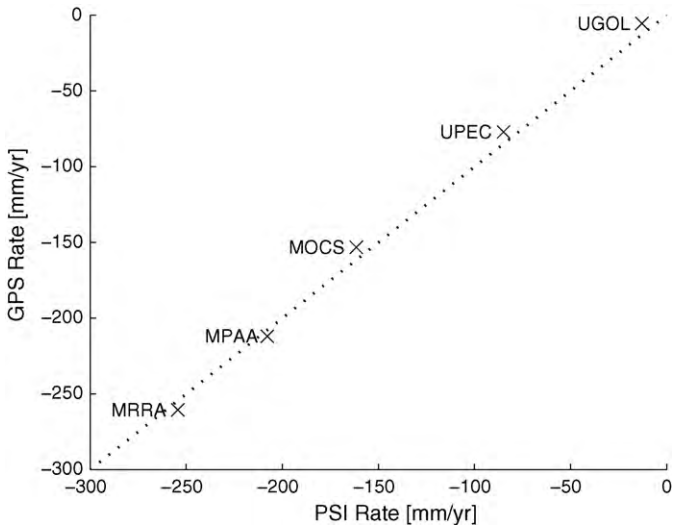

Fig. 10. Subsidence rates obtained using PSI vs. rates obtained from baseline GPS. The dashed line is the 1-to-1 line showing agreement. RMS misfit is 6.9 mm/year.

3.3. PSI Results

PSI rates in the radar line-of-sight direction are shown in Fig. 5. Subsidence rates increase eastwards towards the center of the basin where the clay-rich sediment package is thickest.

A histogram showing the distribution of subsidence rates for the complete PSI dataset (total of 815,070 points) is shown in Fig. 8. 95% of the samples lie between −250.1 and +11.8 mm/year. The distribution clearly has two components. The most common rate is close to zero (±6 mm/year), reflecting stable, non-consolidating lithology in the western part of the city, including volcanic outcrops. The other component reflects subsidence increasing towards the center of the basin.

Fig. 9 compares the subsidence rates from DInSAR (Cabral-Cano et al., 2008) for the period 16 July 1999–7 January 2000, and the current study for the period 16 January 2004–14 July 2006, using similar color scales. The shape of the deforming area in both studies is very similar. Minor differences probably reflect the different time frames for the two datasets, and our choice of UCHI as the velocity reference for the PSI analysis.

3.4. Calibration and validation

It is important to compare the observed deformation rates from different datasets. GPS measurements are independent of the PSI analysis and can be used to estimate the accuracy of PSI measurements. Table 6 lists line-of-sight rates obtained from point-positioning GPS, baseline GPS and PSI analysis. Fig. 10 compares the PSI rate and the GPS baseline data. The root-mean-square (RMS) difference between these two data is 6.9 mm/year.

The differences shown in Table 6 and Fig. 10 reflect the natural variability of the subsidence rates over short distances, different time-spans of the available data, and data noise in each technique. PSI inferred rates indicate differences up to 50 mm/year in a 0.01 km^2 area, i.e. there are high spatial gradients in the actual subsidence rates. We estimate that this effect contributes approximately 2 mm/year uncertainty to the comparison. Even though the subsidence rates do not vary significantly over time, small transient events do occur, precluding long-term extrapolation of the data. GPS rates in Table 6 are calculated over the time-span of the master station data (UCHI), from 22 November 2005 to 31 December 2007, while the PSI data are from 16 January 2004 to 14 July

Please cite this article in press as: Osmanoğlu, B., et al., Mexico City subsidence observed with persistent scatterer InSAR. Int. J. Appl. Earth Observ. Geoinf. (2010), doi:10.1016/j.jag.2010.05.009

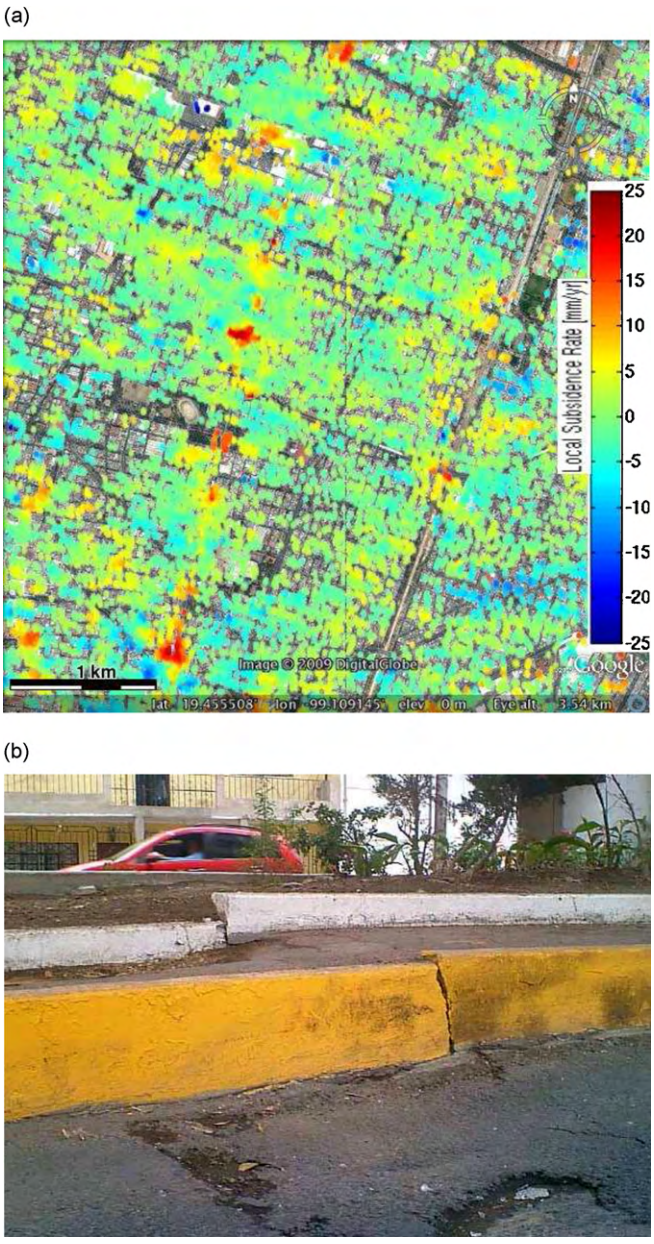

Fig. 11. In this figure, red indicates slower than average subsidence rates, and blue indicates faster than average subsidence. (a) Linear trend (NNW–SSE) of orange to red colors towards the center of the image depict the slower subsidence along the elevated railroad (Metro Line 4, Fig. 1). The differential signal is more pronounced on the metro rail stations (red blobs). (b) Picture taken at the road level underneath the elevated railroad. Offset at the sidewalk (white) is about 15 cm. Dislocation at the curb (yellow) is about 2 cm. (For interpretation of the references to color in this figure legend, the reader is referred to the web version of the article.)

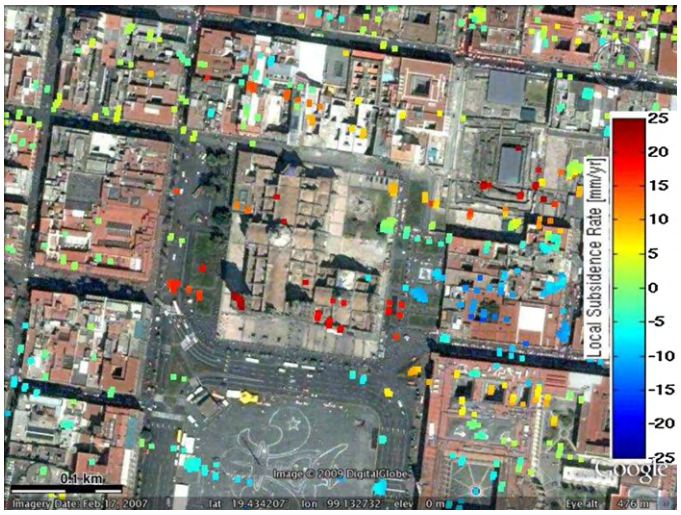

Fig. 12. In this figure, red indicates slower than average subsidence rates, and blue indicates faster than average subsidence. Local subsidence measurements around the Metropolitan Cathedral show slower subsidence on the southern part of the building (red circles). (For interpretation of the references to color in this figure legend, the reader is referred to the web version of the article.)

2006 (Fig. 4). We estimate that the small temporal fluctuation also contributes about 2 mm/year to the comparison.

For displacement or position time series, the precision of a rate estimate is a strong function of the total observing time. For example, using the error model of Mao et al. (1999) for GPS data, Sella et al. (2002) estimate a vertical rate error of about ±5 mm/year after 2 years of observations, declining to about ±2 mm/year after 5 years of observations. For the 2 year time period sampled here, assuming that the PSI has half the error of the GPS (2.5 mm/year) and assuming GPS errors equivalent to Sella et al. (2002) (5 mm/year) we would expect the agreement between PSI and GPS to be approximately $\sqrt{2.5^2 + 5^2 + 2^2 + 2^2} = 6.3$ mm/year, which is very close to the RMS misfit observed in Table 6 and Fig. 10, 6.9 mm/year. If the GPS and PSI errors are assumed to be equal (5 mm/year each), the expected level of agreement becomes 7.6 mm/year. Note that since the GPS-PSI difference (6.9 mm/year) includes real differences due to spatial and temporal variation we can assume that 6.9 mm/year represents an upper bound on the accuracy of the PSI technique for this study.

3.5. Differential deformation

Very high subsidence rates can mask differential motion, mostly due to the limitations of the dynamic range of color scales used on their cartographic display. A better alternative to analyze differential deformation is to calculate an average subsidence rate from neighboring points and subtract this rate from the point of interest (Figs. 11(a) and 12) to obtain a differential subsidence rate. This differential subsidence rate analysis suggests that several civil structures in the study area are experiencing significant differential subsidence along their ground footprint: e.g. Subway Metro Line 4 and the Mexico City Metropolitan Cathedral.

3.5.1. Subway Metro Line 4

This is an elevated metro rail that runs approximately Northeast–Southwest and is supported by vertical columns on horizontal pads. The whole structure is subsiding more slowly than the surrounding area as a result of its overcompensated foundation. Fig. 11 shows the differential deformation along the Metro line and a photograph of deformed pavement along the metro rail.

3.5.2. The Metropolitan Cathedral

The Mexico City Metropolitan Cathedral experiences differential subsidence across its surface footprint (Fig. 1). This is consistent with observations in past decades (Villa et al., 2005). Part of the Cathedral's foundation is located on top of a pre-Hispanic Aztec temple. Preconsolidation of the sediment layer by the earlier temple creates an uneven support to the Cathedral's foundation, causing differential subsidence of the large, heavy masonry structure. Our observations suggest that while the corrective measures performed a few years ago were successful in the general sense, a small difference in subsidence rates spanning the building is still present.

Please cite this article in press as: Osmanoğlu, B., et al., Mexico City subsidence observed with persistent scatterer InSAR. Int. J. Appl. Earth Observ. Geoinf. (2010), doi:10.1016/j.jag.2010.05.009

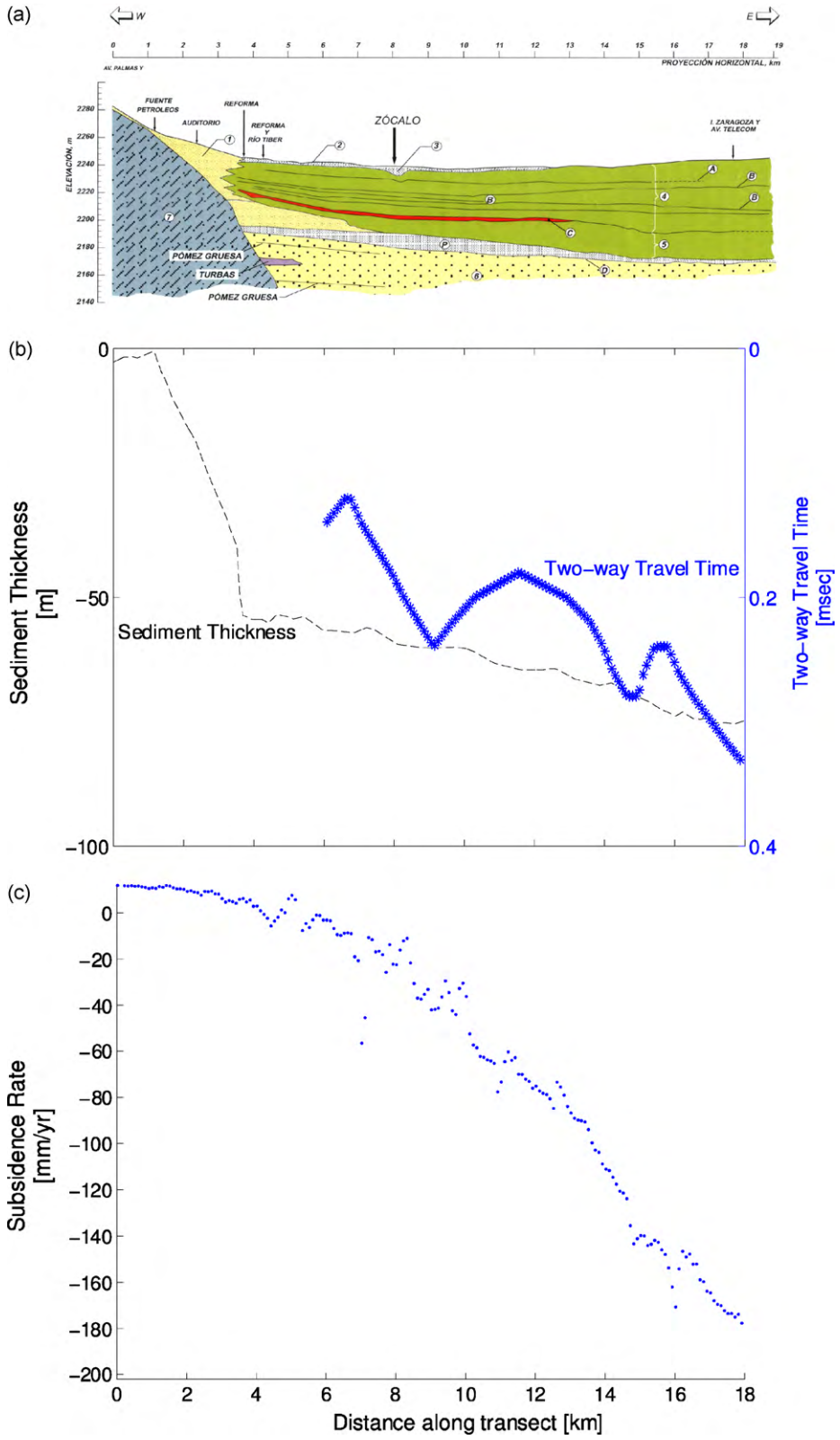

Fig. 13. (a) Geologic cross section of the Mexico City metropolitan area (location shown in Fig. 1) after Villa et al. (2005), (b) sediment thickness (Upper Lacustrine Unit, light green in (a)) derived from direct geotechnical data (black dotted line; Villa et al., 2005) and from geophysical seismic reflection surveys (blue line, Horizon IV; Perez-Cruz, 1988). Thickness of the seismic layer (blue). (c) Observed PSI rates along the cross section profile. (For interpretation of the references to color in this figure legend, the reader is referred to the web version of the article.)

Please cite this article in press as: Osmanoğlu, B., et al., Mexico City subsidence observed with persistent scatterer InSAR. Int. J. Appl. Earth Observ. Geoinf. (2010), doi:10.1016/j.jag.2010.05.009

3.6. Relation between sediment thickness and subsidence rate

Decreasing ground water levels cause consolidation of the clay-rich lacustrine sediments underneath the eastern sector of Mexico City. The high spatial density of the PSI measurements allows study of a possible correlation between subsidence rate and the uppermost sediment layer thickness. We averaged PSI rates within a 250 m wide swath and along an E–W trending geologic cross section (see Figs. 1 and 13a) and compared it to different sediment thickness profiles (Fig. 13b and c). The sediment thickness profiles were obtained from two different sources: (1) a direct subsurface geotechnical data from standard penetration tools (Villa et al., 2005), and (2) a geophysical seismic reflection survey (Perez-Cruz, 1988) tied to deep borehole cores.

Lacustrine sediments prone to extreme consolidation are located within the uppermost 490 m (Perez-Cruz, 1988) throughout the basin. Their thickness shows large spatial variations, but generally increases from the western sector of the city built over the mountain slopes towards the eastern sector of the city, built over the former lacustrine plain. This uppermost stratigraphic unit is commonly referred to as the Upper and Lower Clay Units or alternatively Upper Lacustrine Unit (Horizon IV on Perez-Cruz, 1988).

While Fig. 13a and b shows general agreement between subsidence rate and the overall lacustrine unit thickness, small features in the subsidence data are not reflected in subsurface stratigraphy. This could be explained in several ways. First, geotechnical direct penetration data is inhomogeneously distributed and is largely concentrated along larger civil structures. Second, seismic reflection survey data, are derived from 26 seismic reflection profiles throughout the city, and are interpolated, smoothing out high frequency variation. The lack of correlation at the 4 km mark, where the Upper Lacustrine Unit begins, may indicate that aquifer consolidation involves deeper levels, below the Upper Lacustrine Unit.

4. Conclusion

Observed subsidence rates in Mexico City for the period 2004–2006 using persistent scatterer interferometry (PSI) are very similar to previous studies using other InSAR techniques, with a maximum subsidence rate of 300 mm/year. Comparison with independent GPS measurement rates suggest that the PSI measurements are accurate to better than ±6.9 mm/year.

There is no evidence of significant annual variation in the GPS data, suggesting negligible recharge, and implying continuing degradation and loss of the aquifer underlying Mexico City.

Differences in subsidence rates larger than about 7 mm/year can be effectively imaged using the PSI measurements. This technique has great potential for detecting and predicting structural damage in civil structures due to differential subsidence. Alternatively, the same technique can be used to detect emerging structures with over-compensated foundations.

Acknowledgments

The first author would like to thank NASA for the NESSF Fellowship provided between 2007 and 2009, 09-Earth-09R-61. We thank ESA for providing the Envisat ASAR images through CAT-1 Project #1409 to Enrique Cabral-Cano. We would also like to thank Oscar Diaz-Molina for his invaluable help with the Mexico City GPS network and Edgar Campos Cajero for the photographic coverage of emerging stations of subway Metro Line 4. We also thank Freek van Leijen, Mahmut Arikan and Ramon Hanssen and many others from TU-Delft for making the DORIS and PSI Toolbox available.

References

Altamimi, Z., Sillard, P., Boucher, C., 2002. ITRF2000: a new release of the international terrestrial reference frame for earth science applications. Journal of Geophysical Research (Solid Earth) 107j (October), 1, http://adsabs.harvard.edu/abs/2002JGRB.107j.ETG2A.

Amelung, F., Galloway, D.L., Bell, J.W., Zebker, H.A., Laczniak, R.J., 1999. Sensing the ups and downs of las vegas: InSAR reveals structural control of land subsidence and aquifer-system deformation. Geology 27 (June (6)), 483–486, http://geology.gsapubs.org/cgi/content/abstract/27/6/483.

Argus, D.F., 2007. Defining the translational velocity of the reference frame of earth. Geophysical Journal International 169 (3), 830–838, http://dx.doi.org/10.1111/j.1365-246X.2007.03344.x.

Cabral-Cano, E., Dixon, T.H., Miralles-Wilhelm, F., Diaz-Molina, O., Sanchez-Zamora, O., Carande, R.E., 2008. Space geodetic imaging of rapid ground subsidence in Mexico City. Geological Society of America Bulletin 120 (November (11–12)), 1556–1566, http://gsabulletin.gsapubs.org/cgi/content/abstract/120/11-12/1556.

Carrillo, N., 1947. Influence of artesian wells in the sinking of Mexico City, vol. 47. Secretaria de Hacienda y Credito Publico, Mexico City, pp. 7–14.

Correa-Mora, F., DeMets, C., Cabral-Cano, E., Diaz-Molina, O., 2009. Transient deformation in southern Mexico in 2006 and 2007: evidence for distinct deep-slip patches beneath guerrero and oaxaca. Geochemistry, Geophysics, Geosystems 10 (February (2)).

Correa-Mora, F., Demets, C., Cabral-Cano, E., Marquez-Azua, B., Diaz-Molina, O., 2008. Interplate coupling and transient slip along the subduction interface beneath oaxaca, Mexico. Geophysical Journal International October (175), 269–290, http://adsabs.harvard.edu/abs/2008GeoJI.175.269C.

Cuevas, J., 1936. Foundation conditions in Mexico City. In: Inter. Conf. Soil Mech., vol. 3.

Gobierno del Distrito Federal, 2004. Normas técnicas complementarias para diseño y construcción de cimentaciones: Gaceta Oficial del Distrito Federal, Tomo II, No. 103-BIS, p. 11–39.

Dixon, T.H., Miller, M., Farina, F., Wang, H., Johnson, D., 2000. Present-day motion of the sierra nevada block and some tectonic implications for the basin and range province, North American Cordillera. Tectonics 19, 1–24, http://www.agu.org/pubs/crossref/2000/1998TC001088.shtml.

Ferretti, A., Prati, C., Rocca, F., Inf, D.E., 2001. Permanent scatterers in SAR interferometry. IEEE Transactions on Geoscience and Remote Sensing 39 (1), 8–20.

Freeze, R.A., Cherry, J.A., 1979. Groundwater. Prentice Hall, Inc., Upper Saddle River, NJ, 07458.

Gayol, R., 1929. Breves apuntes relativos a las obras de saneamiento y desague de la capital de la republica y de las que, del mismo genero necesita con urgencia. Revista Mexicana de Ingenieria y Arquitectura VIII.

Gourmelen, N., Amelung, F., Casu, F., Manzo, M., Lanari, R., 2007. Mining-related ground deformation in crescent valley, nevada: implications for sparse gps networks. Geophysical Research Letters May (34), 9309.

Hanssen, R., Bamler, R., 1999. Evaluation of interpolation kernels for SAR interferometry. IEEE Transactions on Geoscience and Remote Sensing January (37), 318–321.

Hanssen, R.F., 2001. Radar Interferometry: Data Interpretation and Error Analysis. Kluwer Academic, Dordrecht.

Hooper, A., Zebker, H., Segall, P., Kampes, B., 2004 December. A new method for measuring deformation on volcanoes and other natural terrains using InSAR persistent scatterers. http://www.agu.org/pubs/crossref/2004/2004GL021737.shtml.

Hong, S.H., Jung, H.S., Won, J.S., Kim, H.G., 2004. Extraction of ground control points (GCPs) from synthetic aperture radar image using DEM. In: Geoscience and Remote Sensing Symposium, 2004. IGARSS'04 Proceedings, vol. 6.

Kampes, B., 2005. Displacement parameter estimation using permanent scatterer interferometry. Ph.D. Thesis, Technische Universiteit Delft.

Kampes, B., Usai, S., 1999. Doris: The delft object-oriented radar interferometric software. In: Proc. 2nd Int. Symp. Operationalization OF Remote Sensing, http://citeseerx.ist.psu.edu/viewdoc/summary?doi=10.1.1.46.1689.

Lanari, R., Lundgren, P., Manzo, M., Casu, F., 2004. Satellite radar interferometry time series analysis of surface deformation for Los Angeles, California. Geophysical Research Letters 31 (December), 23613.

Mao, A., Harrison, C.G.A., Dixon, T.H., 1999. Noise in GPS coordinate time series. Journal of Geophysical Research 104, 2797–2816, http://adsabs.harvard.edu/abs/1999JGR..104.2797M.

Ortega-Guerrero, A., Cherry, J.A., Rudolph, D.L., 1993. Large-Scale aquitard consolidation near Mexico City. Ground Water 31 (5), 708–718, http://dx.doi.org/10.1111/j.1745-6584.1993.tb00841.

Perez-Cruz, G.A., 1988. Estudio sismológico de reflexión del subsuelo de la ciudad de mexico. Master's thesis, Universidad Nacional Autónoma de México, México Distrito Federal.

Poland, J.F., 1984. Guidebook to Studies of Land Subsidence due to Ground-water Withdrawal. UNESCO, Paris.

Scharroo, R., Visser, P., 1998. Precise orbit determination and gravity field improvement for the ers satellites. J. Geophys. Res. 103 (C4), 8113–8127.

Sella, G.F., Dixon, T.H., Mao, A., 2002. REVEL: a model for recent plate velocities from space geodesy. Journal of Geophysical Research 107 (April), http://www.agu.org/pubs/crossref/2002/2000JB000033.shtml.

Small, D., Rosich, B., Meier, E., Nüesch, D., 2004. Geometric calibration and validation of asar imagery. In: Proc. of CEOS SAR Workshop.

Sneed, M., Ikehara, M.E., Stork, S.V., Amelung, F., Galloway, D.L., 2003. Detection and measurement of land subsidence using interferometric synthetic aperture radar

Please cite this article in press as: Osmanoğlu, B., et al., Mexico City subsidence observed with persistent scatterer InSAR. Int. J. Appl. Earth Observ. Geoinf. (2010), doi:10.1016/j.jag.2010.05.009

and global positioning system, San Bernardino County, Mojave Desert, California. Tech. Rep. Water-Resources Investigations Report 03-4015, U.S. Geological Survey, Sacramento, California.
Strozzi, T., Wegmuller, U., 1999. Land subsidence in Mexico City mapped by ERS differential SAR interferometry. In: Geoscience and Remote Sensing Symposium, 1999. IGARSS'99 Proceedings. IEEE 1999 International, vol. 4. pp. 1940–1942.
Strozzi, T., Wegmüller, U., Werner, C., Wiesmann, A., 2002 January. JERS SAR interferometry for land subsidence monitoring. In: Wilson, A., Quegan, S. (Eds.), Retrieval of Bio- and Geo-Physical Parameters from SAR Data for Land Applications, vol. 475 of ESA Special Publication, pp. 145–150.
Terzaghi, K., 1976. Erdbaumechanik auf bodenphysikalischer Grundlage. Gistel & Cie, Vienne.
Villa, E.S., Shelly, E.O., Mooser, F., Plata, E.L., 2005. Sintesis Geotectónica de la Cuenca del Valle de México. TGC Geotecnia, Mexico, D.F.
Webb, F.H., Zumberge, J.F., 1997. An introduction to GIPSY/OASIS-II, Tech. Rep. JPL D-11088. Jet Propulsion Lab., Pasadena, CA.
Zebker, H.A., Villasensor, J., 1992. Decorrelation in interferometric radar echoes. IEEE Transactions on Geoscience and Remote Sensing 30 (September), 950–959, http://adsabs.harvard.edu/abs/1992ITGRS.30.950Z.

Please cite this article in press as: Osmanoğlu, B., et al., Mexico City subsidence observed with persistent scatterer InSAR. Int. J. Appl. Earth Observ. Geoinf. (2010), doi:10.1016/j.jag.2010.05.009